
BiLO: Bilevel Local Operator Learning for PDE inverse problems

Ray Zirui Zhang¹

Xiaohui Xie²

John Lowengrub^{1,3}

¹Department of Mathematics, University of California, Irvine

²Department of Computer Science, University of California, Irvine

³Department of Biomedical Engineering, University of California, Irvine

Abstract

We propose a new neural network based method for solving inverse problems for partial differential equations (PDEs) by formulating the PDE inverse problem as a bilevel optimization problem. At the upper level, we minimize the data loss with respect to the PDE parameters. At the lower level, we train a neural network to locally approximate the PDE solution operator in the neighborhood of a given set of PDE parameters, which enables an accurate approximation of the descent direction for the upper level optimization problem. The lower level loss function includes the L2 norms of both the residual and its derivative with respect to the PDE parameters. We apply gradient descent simultaneously on both the upper and lower level optimization problems, leading to an effective and fast algorithm. The method, which we refer to as BiLO (Bilevel Local Operator learning), is also able to efficiently infer unknown functions in the PDEs through the introduction of an auxiliary variable. Through extensive experiments over multiple PDE systems, we demonstrate that our method enforces strong PDE constraints, is robust to sparse and noisy data, and eliminates the need to balance the residual and the data loss, which is inherent to the soft PDE constraints in many existing methods.

1 Introduction

A fundamental task across various scientific and engineering fields is to infer the unknown parameters of a partial differential equation (PDE) from observed data. Applications include seismic imaging [1–3], electrical impedance tomography [4, 5], personalized medicine [6–9], and climate modeling [10]. PDE inverse problems are commonly addressed within the frameworks of PDE-constrained optimization [11] or Bayesian inference [12]. In the PDE constrained optimization framework, the objective is to minimize the difference between the observed data and the PDE solution, and the PDE is enforced as a constraint using adjoint, or deep learning, methods. In the Bayesian inference framework, the inverse problem is formulated as a statistical inference problem, where the goal is to estimate the posterior distribution of the parameters given the data. This requires sampling parameter space and solving the forward PDE multiple times. Here, we develop a constrained optimization framework for solving PDE inverse problems using deep learning.

1.1 Related work

The **Adjoint Method** is a widely used technique for computing the gradients of the objective function with respect to the PDE parameters using numerical PDE solvers in the PDE-constrained optimization framework. This method provides accurate gradients and strongly satisfies the PDE constraint. However, the method requires explicitly deriving the adjoint equation and solving the forward and adjoint equations at each iteration, which can be complex and computationally expensive [11, 13].

Physics-Informed Neural Networks (PINNs) have emerged as novel methods for solving inverse problems in a PDE constrained optimization framework [7, 14–20]. PINNs represent PDE solutions using neural networks and embed both the data and the PDE into the loss function through a mesh-free approach. By minimizing the total loss, PINNs effectively solve the PDE, fit the data, and infer the parameters simultaneously, showcasing integration of mathematical models with data-driven learning processes. A related approach, **Optimizing a Discrete Loss (ODIL)**, utilizes conventional numerical discretizations of the PDEs and the loss is minimized over the parameters and the PDE solutions at the grid points rather than the weights of a neural network [21, 22]. However, in these methods, the PDE is enforced as a soft constraint, which requires balancing the residual and the data loss, and can lead to a trade-off between fitting the data and solving the PDE accurately.

Operator Learning aims to train neural networks that approximate the PDE solution operator (parameter-to-solution map) and can serve as surrogate models for the forward PDE solvers [23]. Once these surrogates are established, they can be integrated into a Bayesian inference framework or other optimization algorithms to solve inverse problems, leveraging the speed of evaluating a neural network [24–27]. Some examples of operator learning frameworks include the Fourier Neural Operator [28–30], DeepONet [31, 32], In-context operator learning [33], among others, e.g. [5, 34]. However, for solving the inverse problem, neural operators can encounter challenges when the ground truth is out of the distribution of the training dataset.

There are many other methods for PDE inverse problems using deep learning; see [35–37] for more comprehensive reviews.

Main Contributions

In this work, we focus on solving PDE inverse problems in the PDE-constrained optimization framework using deep learning methods. The contributions of this paper are as follows:

- We formulate the PDE inverse problem as a bilevel optimization problem, where the upper level problem minimizes the data loss with respect to the PDE parameters, and the lower level problem involves training a neural network to approximate the PDE solution operator locally at given PDE parameters, enabling approximation of the descent direction for the upper level optimization problem.
- At the lower level problem, we introduce the “residual-gradient” loss, which is the L2 norm of derivative of the residual with respect to the PDE parameters. We show that this loss term compels the neural network to approximate the PDE solution for a small neighborhood of the PDE parameters, thus a “local operator”.
- Extensive experiments over multiple PDE systems demonstrate that our novel formulation is both more accurate and more robust than other existing methods. It exhibits stronger PDE fidelity, robustness to sparse and noisy data, and eliminates the need to balance the residual and the data loss, a common issue in PDE-based soft constraints.
- We solve the bilevel optimization problem using gradient descent simultaneously on both the upper and lower level optimization problems, leading to an effective and fast algorithm. The network architecture is simple and easy to implement.
- We extend our method to infer unknown functions that are also parameterized by neural networks through an auxiliary variable. This bypasses the need to learn a high-dimensional local operator.

Our approach combines elements of PINN, operator learning, and the adjoint method. Our method is closely related to the PINN: both use neural network to represent the solution to the PDE, use automatic differentiation to compute the PDE residual, and aim to solve the PDE and infer the parameters simultaneously. However, in the PINN, the PDE-constraint is enforced as a regularization term (or soft constraint), leading to a trade-off between fitting the data and solving the PDE accurately, which is the main challenge that we aim to address. Compared with operator learning, which solves the PDE for a wide range of parameters and requires a large amount of synthetic data for training, our method only learns the operator local to the PDE parameters at each step of the optimization process and does not require a synthetic dataset for training. Similar to the adjoint method, we aim to approximate the descent direction for the PDE parameters with respect to the data loss. However, we do not require deriving and solving the adjoint equation.

2 Method

2.1 PDE Inverse problem as Bi-level optimization

In this section, we present a novel method for solving PDE inverse problems in the framework of PDE-constrained optimization problems using deep learning. Let $u : \Omega \rightarrow \mathbb{R}$ be a function defined over a domain $\Omega \subset \mathbb{R}^d$ satisfying some boundary conditions, and \hat{u} be the observed data, which might be noisy. Suppose u is governed by a PDE, F , which depends on some parameters Θ . Then the following PDE-constrained optimization problem is solved:

$$\min_{\Theta} \|u - \hat{u}\|_2^2 \quad \text{s.t.} \quad F(D^k u(\mathbf{x}), \dots, Du(\mathbf{x}), u(\mathbf{x}), \Theta) = 0 \quad (1)$$

The constraint is a PDE operator that depends on the parameters Θ . For time-dependent problems, we treat time t as a special component of \mathbf{x} , and Ω includes the temporal domain.

Suppose we know the PDE solution operator (hereafter referred to as the ‘‘operator’’), $u(\mathbf{x}, \Theta)$, which solves the PDE for any Θ , then we can solve the optimization problem easily by minimizing the objective function using a gradient descent algorithm. However, finding the full operator $u(\mathbf{x}, \Theta)$ is challenging and unnecessary. Since we are only interested in the descent direction to update Θ , a local approximation of the solution operator suffices, that is, the operator should approximate the PDE solution for a small neighborhood of a particular value of Θ . For notational simplicity, we define the residual function of the operator as

$$r(\mathbf{x}, \Theta) := F(D^k u(\mathbf{x}, \Theta), \dots, Du(\mathbf{x}, \Theta), u(\mathbf{x}, \Theta), \Theta) \quad (2)$$

If u is a local operator at Θ , then $r(\mathbf{x}, \Theta) = 0$ and $\nabla_{\Theta} r(\mathbf{x}, \Theta) = 0$. Our goal is to approximate the operator locally at Θ using a neural network, and then find the optimal PDE parameters Θ by minimizing the data loss with respect to Θ using a gradient descent algorithm.

Suppose the local operator is parameterized by a neural network $u(\mathbf{x}, \Theta; W)$, where W are the weights of the neural network. The objective function (1) leads to the following data loss:

$$\mathcal{L}_{\text{dat}}(\Theta, W) = \frac{1}{|\mathcal{T}_{\text{dat}}|} \sum_{\mathbf{x} \in \mathcal{T}_{\text{dat}}} |u(\mathbf{x}, \Theta; W) - \hat{u}(\mathbf{x})|^2, \quad (3)$$

where \mathcal{T}_{dat} is the set of collocation points where the data is observed. The residual loss is the L2 norm of the residual function

$$\mathcal{L}_{\text{res}}(W, \Theta) := \frac{1}{|\mathcal{T}_{\text{res}}|} \sum_{\mathbf{x} \in \mathcal{T}_{\text{res}}} |r(\mathbf{x}, \Theta; W)|^2. \quad (4)$$

where \mathcal{T}_{res} is the set of collocation points where the residual loss is evaluated. We introduce the following loss term, the ‘‘residual-gradient loss’’, which is the derivative of the residual with respect to the PDE parameters Θ :

$$\mathcal{L}_{\text{rgrad}}(\Theta, W) = \frac{1}{|\mathcal{T}_{\text{res}}|} \sum_{\mathbf{x} \in \mathcal{T}_{\text{res}}} |\nabla_{\Theta} r(\mathbf{x}, \Theta)|^2, \quad (5)$$

Intuitively, this loss compels the neural network to approximate the PDE solution for a small neighborhood of Θ : small variation of Θ should only lead to small variation of the residual. If this is satisfied, then the derivative of the data loss with respect to Θ will approximate the descent direction, and we can find the optimal Θ by minimizing the data loss with respect to Θ using a gradient descent algorithm. We define the ‘‘local operator loss’’ as the sum of the residual loss and the residual-gradient loss with weight w_{rgrad} :

$$\mathcal{L}_{\text{LO}}(\Theta, W) = \mathcal{L}_{\text{res}}(\Theta, W) + w_{\text{rgrad}} \mathcal{L}_{\text{rgrad}}(\Theta, W) \quad (6)$$

Finally, we propose to solve the following bilevel optimization problem:

$$\begin{cases} \Theta^* = \arg \min_{\Theta} \mathcal{L}_{\text{dat}}(\Theta, W^*(\Theta)) \\ W^*(\Theta) = \arg \min_W \mathcal{L}_{\text{LO}}(\Theta, W) \end{cases} \quad (7)$$

In the upper level problem, we find the optimal PDE parameters Θ by minimizing the data loss with respect to Θ . In the lower level problem, we train a network to approximate the local operator $u(\mathbf{x}, \Theta; W)$ by minimizing the local operator loss with respect to the weights of the neural network.

Pre-train and Fine-tune In this work, we assume access to an initial guess of the PDE parameters, Θ_0 , alongside their corresponding numerical solution, denoted as u_0 , e.g. from the finite difference method. The numerical solutions are computed with high accuracy on fine grids, and can be considered as the “exact” solution of the PDE. We can use the numerical solution to pre-train the neural network, and then use the data to fine-tune the neural network to infer the PDE parameters. This has been successfully applied in [7], and is also similar to curriculum learning, where the neural network learns a “simpler” PDE solution first [38]. We define the pre-training data loss \mathcal{L}_{u_0} , which is the MSE between the numerical solution u_0 and the local operator at Θ_0 :

$$\mathcal{L}_{u_0}(W) = \frac{1}{|\mathcal{T}_{\text{res}}|} \sum_{\mathbf{x} \in \mathcal{T}_{\text{res}}} |u(\mathbf{x}, \Theta_0; W) - u_0(\mathbf{x})|^2, \quad (8)$$

In the pre-training phase, we solve the following minimization problem

$$\min_W \mathcal{L}_{\text{LO}}(\Theta_0, W) + \mathcal{L}_{u_0}(W) \quad (9)$$

The use of \mathcal{L}_{u_0} is not mandatory for training the local operator with fixed Θ_0 , though it can speed up the training process.

2.2 Inferring an unknown function

We can also extend our method to learn an unknown function $f(\mathbf{x})$ in the PDE, such as a variable diffusion coefficient in the Poisson equation or an initial condition in the heat equation. In these cases, the following PDE constrained optimization problem is solved:

$$\min_f \|u - \hat{u}\|^2 + w_{\text{reg}} \|\nabla f\|^2 \quad \text{s.t.} \quad F(D^k u(\mathbf{x}), \dots, Du(\mathbf{x}), u(\mathbf{x}), f(\mathbf{x})) = 0 \quad (10)$$

where the constraint is a PDE that depends on the unknown function f . Given that these problems are ill-posed, regularization of the unknown function is often necessary. A typical choice is an L2-norm of the gradient of the unknown function, which penalizes functions that are not smooth. While the selection of an appropriate regularization form is critical, this paper assumes such choices are predetermined, not an aspect of the method under direct consideration.

Suppose f is parameterized by a neural network $f(\mathbf{x}; V)$ with weights V . A straightforward extension from the scalar parameter case is to learn the local operator of the form $u(\mathbf{x}, V)$. However, this would be computationally expensive, as the weights V can be very high dimensional. We propose to introduce an auxiliary variable $z = f(\mathbf{x})$, and find a local operator $u(\mathbf{x}, z)$ such that $u(\mathbf{x}, f(\mathbf{x}))$ solves the PDE locally at f . We define the following function a , which is the residual function with an auxiliary variable z :

$$a(\mathbf{x}, z) := F(D^k u(\mathbf{x}, z), \dots, Du(\mathbf{x}, z), u(\mathbf{x}, z), z) \quad (11)$$

If u is a local solution operator at f , then we should have $a(\mathbf{x}, f(\mathbf{x})) = 0$ and $\nabla_z a(\mathbf{x}, f(\mathbf{x})) = 0$.

Suppose f and u are parameterized by neural networks: $f(\mathbf{x}; V)$ and $u(\mathbf{x}; W)$. The data loss is similar to the parameter inference case (3) and depends on both V and W . We also need the regularization loss, evaluated on \mathcal{T}_{reg} :

$$\mathcal{L}_{\text{reg}}(V) = \frac{1}{|\mathcal{T}_{\text{reg}}|} \sum_{\mathbf{x} \in \mathcal{T}_{\text{reg}}} |\nabla_{\mathbf{x}} f(\mathbf{x}; V)|^2. \quad (12)$$

We define the residual loss:

$$\mathcal{L}_{\text{res}}(W, V) := \frac{1}{|\mathcal{T}_{\text{res}}|} \sum_{\mathbf{x} \in \mathcal{T}_{\text{res}}} |a(\mathbf{x}, f(\mathbf{x}; V); W)|^2. \quad (13)$$

and the residual-gradient loss:

$$\mathcal{L}_{\text{rgrad}}(W, V) = \frac{1}{|\mathcal{T}_{\text{res}}|} \sum_{\mathbf{x} \in \mathcal{T}_{\text{res}}} |\nabla_z a(\mathbf{x}, f(\mathbf{x}; V); W)|^2 \quad (14)$$

This has the same interpretation as the parameter inference case (5): small variation of f should lead to small variation of the residual. Finally, we solve the following bilevel optimization problem:

$$\begin{cases} V^* = \arg \min_V \mathcal{L}_{\text{dat}}(W^*(V), V) + w_{\text{reg}} \mathcal{L}_{\text{reg}}(V) & (15) \\ W^*(V) = \arg \min_W \mathcal{L}_{\text{LO}}(W, V) & (16) \end{cases}$$

where $\mathcal{L}_{\text{LO}} = \mathcal{L}_{\text{res}} + w_{\text{rgrad}}\mathcal{L}_{\text{rgrad}}$. At the upper level, we minimize the data loss and the regularization loss with respect to the weights V of the unknown function, and at the lower level, we minimize the local operator loss with respect to the weights W of the local operator. The pre-training stage is similar to the parameter inference case. Given an initial guess of the unknown function f_0 , and its corresponding numerical solution u_0 , we can train the network f_V to approximate f_0 by minimizing the MSE between f_V and f_0 , and train the network u_W to be the local operator at f_0 by minimizing the local operator loss and the MSE between u_W and u_0 .

2.3 Algorithm

The network architecture involves a simple modification at the input layer (embedding layer) of the typical fully connected neural network: the embedding of the PDE parameters Θ is randomly initialized and fixed during training, so that the residual-gradient loss can not be made 0 by setting the embedding to 0. See Appendix A for more details.

Solving a bilevel optimization problem is challenging in general [39]. In our case, the upper level problem (PDE inverse problem) is usually non-convex, and the lower level problem has a challenging loss landscape [38, 40]. However, the lower level problem does not need to be solved to optimality at each iteration because the primary goal is to approximate the descent direction for the upper level problem. We propose to apply gradient descent to the upper and lower level optimization problems simultaneously. In Algorithm. 1, we describe our optimization algorithm for inferring scalar parameters in the BiLO framework. The algorithm for inferring unknown functions is similar. We write the algorithm as simple gradient descent for notational simplicity while in practice we use the ADAM optimizer [41].

Algorithm 1 Bi-level Local Operator for inferring scalar PDE parameters

- 1: **Input:** Collections of collocation points \mathcal{T}_{res} and \mathcal{T}_{dat} , initial guess of the PDE parameters Θ_0 and the corresponding numerical solution u_{FDM} .
- 2: **Pre-train:** Solve the following minimization problem

$$\min_W \mathcal{L}_{\text{LO}}(\Theta_0, W) + \mathcal{L}_{u_0}(W)$$

- 3: **Fine-Tune:** Simultaneous gradient descent at the upper and lower level (7).

$$\begin{cases} \Theta^{k+1} = \Theta^k - lr_{\Theta} \nabla_{\Theta} \mathcal{L}_{\text{dat}}(\Theta^k, W^k) & (17) \\ W^{k+1} = W^k - lr_W \nabla_W \mathcal{L}_{\text{LO}}(\Theta^k, W^k) & (18) \end{cases}$$

We can have two different learning rates for the two groups of variables W and Θ , denoted as lr_W and lr_{Θ} , respectively. We empirically determined $w_{\text{rgrad}} = 1e - 3$ and $lr_W = lr_{\Theta} = 0.001$ to be effective across our numerical experiments. It is not imperative for the residual-gradient loss to be minimized excessively; it is sufficient that it approximate the correct descent direction. Under somewhat restrictive assumptions, we are able to obtain a theoretical characterization of the bilevel optimization problem (shown below. See Appendix B for a proof). A more general theoretical understanding of the learning dynamics is still lacking and will be left for future work.

Proposition: Assuming (i) the maximum principal holds for the PDE operator; (ii) the parametrized local operator $u(W, \Theta) = g$ on $\partial\Omega$ for all W and Θ ; (iii) the lower level problem has a minimizer $W^*(\Theta)$ such that the $u(W^*(\Theta), \Theta)$ is the local operator, then the approximate gradient of the upper level objective at $W^*(\Theta)$ is exact.

2.4 Difference between PINNs and Neural Operators for inverse problems

Neural Operator Neural operators can serve as surrogate models for PDE solution operators, and can be used in algorithms that require solving the forward PDE multiple times, such as Bayesian inference or derivative-free optimization [26, 42], or gradient-based optimization algorithms [26, 43, 44]. However, if the objective is to estimate parameters from limited data, the considerable initial cost for data generation and network training might seem excessive. The accuracy of specific PDE solutions depends on the accuracy of the neural operator, and which may decrease if the true PDE

parameters fall outside the training data’s distribution [45]. This issue can be mitigated by instance-wise fine-tuning using the residual loss [29, 32], though it introduces an additional trade-off: fine-tuning for one parameter set could reduce the operator’s overall accuracy for other parameters. (an “anchor loss” is thus required to maintain generalization [29]). Thus, in the context of finding the best estimate of the parameters given the data in a PDE-constrained optimization framework, we mainly compare BiLO with PINNs.

PINN Within the PINN framework, the solution of the PDE is represented by a deep neural network $u(\mathbf{x}, W)$, where W denotes all the trainable weights of the neural network [14, 15, 46]. Notice that the PDE parameters Θ are not part of the network input. Therefore the data loss does not depend on the PDE parameters Θ , and we write the data loss as $\mathcal{L}_{\text{dat}}(W)$. and the residual loss depends on the weights of the neural network and the PDE parameters.

Solving an inverse problem using PINN involves minimizing an unconstrained optimization problem, where the objective function is the weighted sum of the residual loss and the data loss

$$\min_{W, \Theta} \mathcal{L}_{\text{res}}(W, \Theta) + w_{\text{dat}} \mathcal{L}_{\text{dat}}(W) \quad (19)$$

where w_{dat} is the weight of the data loss. For simplicity of discussion, we assume the weight of the residual loss is always 1. The key feature is that the PDE is enforced as a soft constraint, or as a regularization term for fitting the data. The relationship between the PDE parameter and the data loss is indirect: the descent directions of the PDE parameters are given by $\nabla_{\Theta} \mathcal{L}_{\text{res}}$, which are independent of the data loss.

Challenges for PINNs Solving PDE inverse problems using PINNs can encounter challenges stemming from the soft PDE constraint (19), especially when the data is sparse and noisy, or when the PDE model does not fully explain the data. The soft PDE constraint can result in a trade-off between fitting the data and solving the PDE accurately. In addition, since the PDE parameters are updated in the descent direction of the residual loss, they can be biased toward parameters corresponding to very smooth solutions. This can also lead to slow convergence, as a small residual loss can be achieved by any PDE parameters corresponding to a smooth solution, and the step size can become small before the data loss is sufficiently minimized. It is important to recognize that PINNs can indeed be effective for PDE inverse problems, particularly when the data is abundant and the noise is independent and identically distributed: in this case, the minimizer of the data loss still gives a good approximation of the PDE solution [17, 18, 20]. The challenges become more pronounced with sparse and noisy data or misspecified models [7].

There are many techniques to improve the performance of PINNs, such as adaptive sampling and weighting of collocation points [46–49], new architectures [50–53], new optimization algorithms [38, 54], new loss functions [55–57], adaptive weighting of loss terms [52, 58–60]. While most of these techniques focus on the forward problem, they can potentially be used for inverse problem as well. However, these techniques do not fundamentally change the soft PDE-constraints in the PINN framework. In our work, we propose a different optimization problem that does not involve a trade-off between the residual loss and the data loss, and our method can be used in conjunction with many of these techniques to improve the performance. Therefore, in the following numerical experiments, we do not use any of these techniques, and we focus on comparing the two different optimization formulations (bi-level optimization and the soft PDE-constraints).

3 Numerical Experiments

In Section 3.1, we infer two scalar parameters in the Fisher-KPP equation and compare the performance of BiLO, PINN and DeepONet. In Section 3.2, we infer an unknown function in the Poisson equation and compare the performance of BiLO and PINN (results of DeepONet are shown in Appendix D.2). We denote the neural network solution (from BiLO, PINN, or DeepONet) by u_{NN} , and denote the numerical solution with the inferred parameters using the Finite Difference Method (FDM) by u_{FDM} , which is solved to a high accuracy. A large discrepancy between u_{NN} and u_{FDM} suggests that the PDE is not solved accurately by the neural network.

We provide the training detail and hyperparameters for the numerical experiments in Section 3.1 and 3.2 in Appendix C. Details of the DeepONet architecture and training are provided in Appendix D. Appendix E provides additional numerical experiments: (1) E.1 Inferring a scalar coefficient

cient in a nonlinear ODE problem; (2) E.2 Inferring the initial condition of a 1D heat equation; (3) E.3 Inferring the variable diffusion coefficient of a 2D Poisson problem, where we achieve better or comparable performance as in PINO [29].

3.1 Fisher-KPP Equation

In this example, we aim to infer the unknown parameters D and ρ in the following Fisher-KPP equation [61], which is a nonlinear reaction-diffusion equation:

$$\begin{cases} u_t(x, t) = 0.01Du_{xx}(x, t) + \rho u(1 - u) \\ u(x, 0) = \frac{1}{2} \sin(\pi x)^2 \\ u(0, t) = u(1, t) = 0 \end{cases} \quad (20)$$

The initial guesses of the PDE parameters are $D_0 = 1$ and $\rho_0 = 1$, and the ground truth parameters are $D_{GT} = 2$ and $\rho_{GT} = 2$. This equation has been used to model various biological phenomena, such as the growth of tumors [62, 63] or the spreading of misfolded proteins [8, 64, 65]. In our tests the data is only provided at the final time $t = 1$, which is more challenging than the case where data is provided at multiple time points. This single-time inference problem has application in patient-specific parameter estimation of tumor growth models using medical images, where only one time point may be available, e.g., in the case of glioblastoma [7, 22, 66, 67].

Effect of residual-gradient loss We plot the trained local operator $u(\mathbf{x}, D_0 + \delta D, \rho_0 + \delta \rho; W)$ at $t = 1$, for $(\delta D, \delta \rho) = (0.5, 0)$ and $(0, 0.1)$, and the corresponding FDM solution in Fig. 1 (a). We can see that even though the network is only trained using the initial parameters, because of the residual-gradient loss, the network can approximate the solution of the PDE for a small neighborhood of the parameters. This suggests that the derivative of the data loss with respect to the parameters should give the correct descent direction.

Trajectory of the Parameters We consider the case without noise and show the trajectories of the parameters D and ρ during the fine-tuning process in Fig. 1 (b). Each BiLO trajectory (black line) corresponds to a different random initialization of the neural network, and are obtained by our simultaneous gradient descent. They roughly follow the trajectory that is obtained by solving the lower level problem to a small tolerance before updating the PDE parameters (red dashed line). The contours are the data loss in log scale using the FDM solution for each parameter pair (D, ρ) . Note that the contour lines do not represent the actual loss landscape of our optimization problem, since at each step we are not solving the PDE to high accuracy. From the landscape we can also see that single-time inference is challenging, as the gradient with respect to D is much smaller than ρ , leading to a narrow valley in the loss landscape along the D -direction.

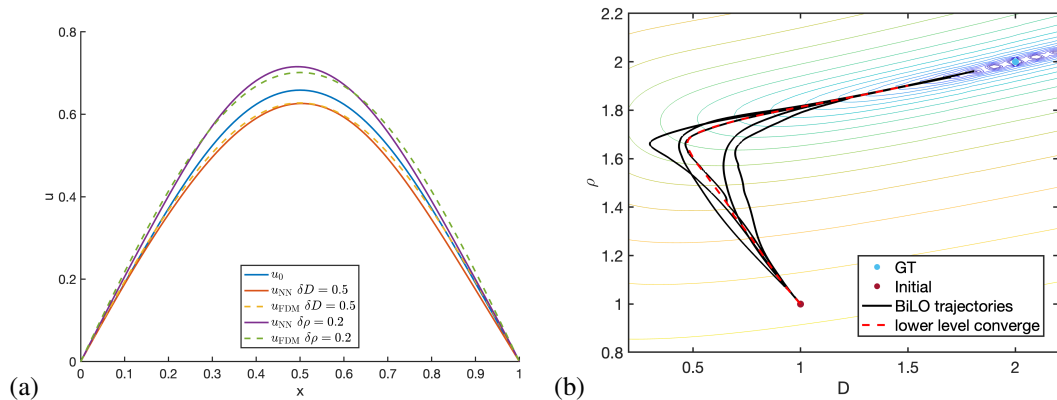


Figure 1: (a) Visualization of the local operator $u(\mathbf{x}, D_0 + \delta D, \rho_0 + \delta \rho; W)$ at $t = 1$ for $\delta D = 0.5$ or $\delta \rho = 0.2$, and the corresponding FDM solutions. (b) Trajectory of the parameters D and ρ during fine-tuning roughly follow the path of the steepest descent. The dashed line is the trajectory when the lower level problem is solved to a small tolerance. The contours correspond to the data loss in log scale, computed using the FDM solution.

Inference with noise In this experiment, we consider inference under noise $\epsilon \sim N(0, 1e - 4)$. In Fig. 2, we show the results of BiLO and PINNs with different weights $w_{\text{dat}} = 0.01, 0.1, 1$. We can see

that for $w_{\text{dat}} = 0.01$ and 0.1 , the PDE is solved relatively accurately, since u_{NN} and u_{FDM} overlap. For $w_{\text{dat}} = 1$, the PDE is not solved accurately and the network is over-fitting the data. In addition, PINNs have difficulties in obtaining accurate estimates of D due to the challenging loss landscape. Our new method gives more accurate inferred parameter and PDE solution.

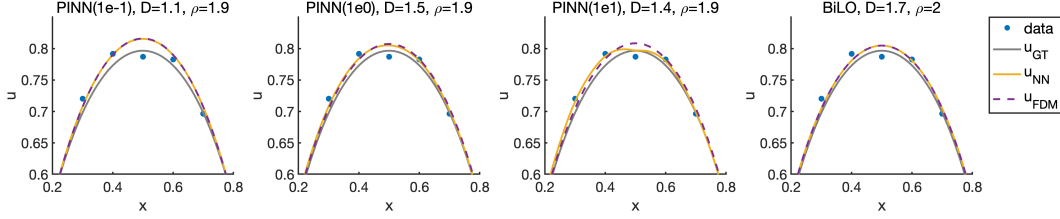


Figure 2: Enlarged view of the network predicted solutions u_{NN} (BiLO and PINNs with different w_{dat}) and FDM solutions u_{FDM} at final time, in the region $(x, u) \in [0.2, 0.8] \times [0.6, 0.85]$. BiLO gives more accurate inferred parameters and PDE solution.

In Table 1, we show the mean and standard deviation (std) of various metrics for BiLO, PINNs with different w_{dat} , and DeepONets with different pretraining datasets. The ground truth solution should have an average data loss of $\mathcal{L}_{\text{dat}} = 1e - 4$, which is the variance of the noise. We can see that the loss landscape is particularly challenging, leading to relatively large error in D for all methods. For the PINN, we see that $w_{\text{dat}} = 0.01$ leads to under-fitting of the data, as the data loss is larger than the variance of the noise; and $w_{\text{dat}} = 10$ shows clear sign of over-fitting of the data, as the data loss is getting smaller than the variance of the noise. The DeepONets are first pretrained with numerical solutions of the PDE with various D and ρ . Then a gradient-based optimization algorithm is used to solve the inverse problem. We consider both coarse and dense sampling of the parameters D and ρ that include the ground truth parameters. Additionally, we also consider a dense sampling but the ground truth parameters are out-of-distribution(OOD). Details are provided in Appendix. D.1. We can see that the results from DeepONet are affected by the quality of the pretraining dataset. Overall, BiLO gives more accurate inferred parameters and PDE solution, is robust to the noise, and does not require a large amount of pretraining data.

method	$ D - D_{GT} $	$ \rho - \rho_{GT} $	$\ u_{\text{NN}} - u_{\text{FDM}}\ _{\infty}$	$\mathcal{L}_{\text{data}}$
BiLO	0.26±0.10	0.06±0.03	3.36e-3±1.14e-3	1.01e-4±2.77e-5
PINN(1e-1)	0.85±0.07	0.17±0.02	9.40e-3±9.15e-4	1.43e-4±2.58e-5
PINN(1e0)	0.40±0.13	0.09±0.03	4.41e-3±1.44e-3	8.68e-5±3.00e-5
PINN(1e1)	0.44±0.21	0.10±0.04	4.93e-3±2.10e-3	3.29e-5±2.02e-5
DeepONet(Coarse)	0.95±0.74	0.24±0.20	7.96e-3±6.36e-3	6.26e-5±2.81e-5
DeepONet(Dense)	0.48±0.40	0.13±0.10	4.85e-3±3.47e-3	6.23e-5±1.95e-5
DeepONet(OOD)	0.95±0.86	0.35±0.38	1.62e-2±1.75e-2	6.18e-5±1.88e-5

Table 1: Comparison of BiLO, PINNs (with various w_{dat}) and DeepONet (with various pretraining dataset) for a Fisher-KPP PDE problem with noise $\epsilon \sim N(0, 1e - 4)$. BiLO gives more accurate inferred parameters and PDE solution.

3.2 Poisson Equation with Variable Diffusion Coefficient

In this test, we consider the following Poisson equation on $[0, 1]$ with $u(0) = u(1) = 0$:

$$(D(x)u'(x))' = -\pi^2 \sin(\pi x) \quad (21)$$

and aim to infer the variable diffusion coefficient $D(x)$ such that $D(0) = D(1) = 1$. The ground truth $D(x)$ is a ‘‘hat’’ function $D(x) = 1 + 2x$ for $x \in [0, 0.5]$ and $D(x) = 2 - 2x$ for $x \in [0.5, 1]$. We start with initial guess $D_0(x) = 1$.

Effect of residual-gradient loss In Fig. 3, we visualize the local operator $u(x, z; W)$ after pre-training with $D_0(x) = 1$. We consider the variation $\delta D_1(x) = -0.1$, and $\delta D_2(x) = 0.1x$ and evaluate the neural network at $u(x, D_0(x) + \delta D_i(x); W)$ for $i = 1, 2$. The FDM solutions of the PDE corresponding to $D_0(x) + \delta D_i(x)$ are also plotted. We can see that the neural network approximates the solution corresponding to $D_0(x) + \delta D_i(x)$ well.

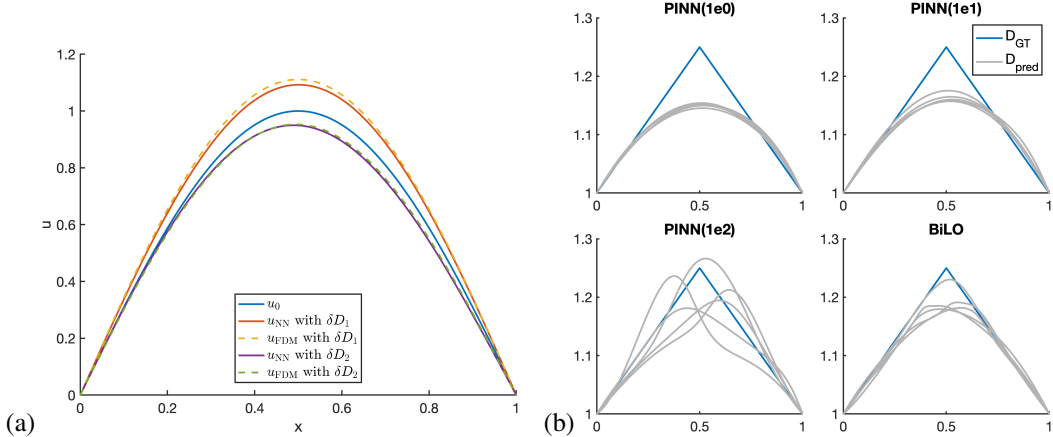


Figure 3: (a) Visualizing the operator $u(x, D(x) + \delta D(x); W)$ after pre-training with $D_0(x) = 1$. (b) Inferred $D(x)$ using noisy data with 5 random seeds: BiLO and PINN with various w_{dat} . BiLO gives more accurate inferred $D(x)$.

method	$\ D - D_{GT}\ _\infty$	$\ D - D_{GT}\ _2$	$\ u_{\text{NN}} - u_{\text{FDM}}\ _\infty$	$\mathcal{L}_{\text{data}}$
BiLO	5.86e-2±1.99e-2	2.01e-2±7.94e-3	3.94e-3±1.93e-3	1.01e-4±1.80e-5
PINN(1e0)	9.99e-2±2.88e-3	3.97e-2±1.73e-3	6.37e-3±1.54e-3	1.09e-4±1.85e-5
PINN(1e1)	8.61e-2±7.50e-3	3.25e-2±3.96e-3	4.43e-3±1.37e-3	1.02e-4±1.87e-5
PINN(1e2)	7.13e-2±1.59e-2	3.11e-2±1.09e-2	4.88e-3±1.45e-3	9.42e-5±1.55e-5

Table 2: Comparison of BiLO and PINNs with various w_{dat} for inferring a variable diffusion coefficient from noisy data. BiLO is more robust to the noise and gives a more accurate inferred diffusion coefficient and PDE solution.

Inference With Noise Data In this experiment, we consider inference under noise $\epsilon \sim N(0, 1e-4)$ and set $w_{\text{reg}} = 1e-3$. In Table. 2, we show the mean and standard deviation of various metrics. We consider the L_∞ and L_2 error of the inferred function $D(x)$ from the ground truth D_{GT} , which measure the accuracy of the inferred function; The L_∞ error between u_{NN} and u_{FDM} indicates the accuracy of neural network solution; We also show the average data loss \mathcal{L}_{dat} , which ideally should be close to the variance of the noise ($1e-4$). A smaller or larger average \mathcal{L}_{dat} indicates tendencies to under-fitting or over-fitting of the data. For the PINNs, we can see that the optimal w_{dat} is about 10, as increasing to 100 leads to over-fitting of the data, and decreasing to 0.1 leads to under-fitting of the data. BiLO results in more accurate inferred diffusion coefficient and PDE solution, and is robust to the noise. We also visualize the inferred $D(x)$ in Fig. 3 (b). For the PINN, we can see that a small w_{dat} leads to very smooth $D(x)$, while a large w_{dat} leads to an oscillating $D(x)$ due to over-fitting. BiLO gives more accurate inferred $D(x)$ that better approximate the kink of the ground truth $D(x)$. In Appendix. D.2, we also compare BiLO with DeepONet, whose performance depends on the pretraining dataset.

4 Conclusion

In this work, we propose a Bi-level Local Operator (BiLO) learning framework for solving PDE inverse problems: we minimize the data loss with respect to the PDE parameters at the upper level, and learn the local solution operator of the PDE at the lower level. The bi-level optimization problem is solved using simultaneous gradient descent, leading to an efficient algorithm. Empirical results demonstrate more accurate parameter recovery and stronger fidelity to the underlying PDEs under sparse and noisy data, compared with the soft PDE-constraint formulation, which faces the delicate trade-off between adhering to the PDE constraints and accurately fitting the data. As **limitations**: (1) the convergence results are mainly empirical with limited theoretical analysis, (2) the numerical experiments are limited to low dimensional problems, and (3) the architecture of the neural network is simple. Future work includes theoretical analysis of the method, applying the method to more complex and higher dimensional problems, and improving the network architectures.

Code Availability

The code for the numerical experiments is available at <https://github.com/Rayzhangzirui/BILO>.

Acknowledgment

R.Z.Z and J.S.L thank Babak Shahbaba for the GPU resources.

References

- [1] Chengyuan Deng et al. *OpenFWI: Large-Scale Multi-Structural Benchmark Datasets for Seismic Full Waveform Inversion*. June 23, 2023. arXiv: 2111.02926 [cs, eess]. URL: <http://arxiv.org/abs/2111.02926>. preprint.
- [2] James Martin et al. “A Stochastic Newton MCMC Method for Large-Scale Statistical Inverse Problems with Application to Seismic Inversion”. In: *SIAM Journal on Scientific Computing* 34.3 (Jan. 2012), A1460–A1487.
- [3] Yan Yang et al. “Seismic Wave Propagation and Inversion with Neural Operators”. In: *The Seismic Record* 1.3 (Nov. 2, 2021), pp. 126–134.
- [4] G. Uhlmann. “Electrical Impedance Tomography and Calderón’s Problem”. In: *Inverse Problems* 25.12 (Dec. 2009), p. 123011.
- [5] Roberto Molinaro et al. *Neural Inverse Operators for Solving PDE Inverse Problems*. June 3, 2023. arXiv: 2301.11167 [math-ph]. URL: <http://arxiv.org/abs/2301.11167>. preprint.
- [6] Jana Lipková et al. “Personalized Radiotherapy Design for Glioblastoma: Integrating Mathematical Tumor Models, Multimodal Scans, and Bayesian Inference”. In: *IEEE Transactions on Medical Imaging* 38.8 (Aug. 2019), pp. 1875–1884.
- [7] Ray Zirui Zhang et al. *Personalized Predictions of Glioblastoma Infiltration: Mathematical Models, Physics-Informed Neural Networks and Multimodal Scans*. Jan. 23, 2024. arXiv: 2311.16536 [cs, eess, q-bio]. URL: <http://arxiv.org/abs/2311.16536>. preprint.
- [8] Amelie Schäfer et al. “Bayesian Physics-Based Modeling of Tau Propagation in Alzheimer’s Disease”. In: *Frontiers in Physiology* 12 (July 16, 2021), p. 702975. pmid: 34335308.
- [9] Shashank Subramanian et al. “Ensemble Inversion for Brain Tumor Growth Models With Mass Effect”. In: *IEEE Transactions on Medical Imaging* 42.4 (Apr. 2023), pp. 982–995.
- [10] Mrinal K. Sen and Paul L. Stoffa. *Global Optimization Methods in Geophysical Inversion*. Cambridge: Cambridge University Press, 2013.
- [11] Michael Hinze et al. *Optimization with PDE Constraints*. Springer Science & Business Media, Oct. 16, 2008. 279 pp. Google Books: Pfbqxa2uDS8C.
- [12] A. M. Stuart. “Inverse Problems: A Bayesian Perspective”. In: *Acta Numerica* 19 (May 2010), pp. 451–559.
- [13] R.-E. Plessix. “A Review of the Adjoint-State Method for Computing the Gradient of a Functional with Geophysical Applications”. In: *Geophysical Journal International* 167.2 (Nov. 1, 2006), pp. 495–503.
- [14] George Em Karniadakis et al. “Physics-Informed Machine Learning”. In: *Nature Reviews Physics* 3.6 (6 June 2021), pp. 422–440.
- [15] M. Raissi, P. Perdikaris, and G. E. Karniadakis. “Physics-Informed Neural Networks: A Deep Learning Framework for Solving Forward and Inverse Problems Involving Nonlinear Partial Differential Equations”. In: *Journal of Computational Physics* 378 (Feb. 1, 2019), pp. 686–707.
- [16] Ameya D. Jagtap, Dimitrios Mitsotakis, and George Em Karniadakis. “Deep Learning of Inverse Water Waves Problems Using Multi-Fidelity Data: Application to Serre–Green–Naghdi Equations”. In: *Ocean Engineering* 248 (Mar. 15, 2022), p. 110775.
- [17] Ameya D. Jagtap et al. “Physics-Informed Neural Networks for Inverse Problems in Supersonic Flows”. In: *Journal of Computational Physics* 466 (Oct. 1, 2022), p. 111402.

- [18] Yuyao Chen et al. “Physics-Informed Neural Networks for Inverse Problems in Nano-Optics and Metamaterials”. In: *Optics Express* 28.8 (Apr. 13, 2020), pp. 11618–11633.
- [19] Liu Yang, Xuhui Meng, and George Em Karniadakis. “B-PINNs: Bayesian Physics-Informed Neural Networks for Forward and Inverse PDE Problems with Noisy Data”. In: *Journal of Computational Physics* 425 (Jan. 15, 2021), p. 109913.
- [20] Taniya Kapoor et al. “Physics-Informed Neural Networks for Solving Forward and Inverse Problems in Complex Beam Systems”. In: *IEEE Transactions on Neural Networks and Learning Systems* (2024), pp. 1–15. arXiv: 2303.01055 [cs, math].
- [21] Petr Karnakov, Sergey Litvinov, and Petros Koumoutsakos. *Optimizing a Discrete Loss (ODIL) to Solve Forward and Inverse Problems for Partial Differential Equations Using Machine Learning Tools*. May 9, 2022. arXiv: 2205.04611 [physics]. URL: <http://arxiv.org/abs/2205.04611>. preprint.
- [22] Michal Balcerak et al. *Individualizing Glioma Radiotherapy Planning by Optimization of Data and Physics-Informed Discrete Loss*. Feb. 25, 2024. arXiv: 2312.05063 [physics, q-bio]. URL: <http://arxiv.org/abs/2312.05063>. preprint.
- [23] Nikola Kovachki et al. *Neural Operator: Learning Maps Between Function Spaces*. Oct. 6, 2022. arXiv: 2108.08481 [cs, math]. URL: <http://arxiv.org/abs/2108.08481>. preprint.
- [24] Tingtao Zhou et al. *AI-aided Geometric Design of Anti-infection Catheters*. Apr. 27, 2023. arXiv: 2304.14554 [cond-mat, physics:physics]. URL: <http://arxiv.org/abs/2304.14554>. preprint.
- [25] Jaideep Pathak et al. *FourCastNet: A Global Data-driven High-resolution Weather Model Using Adaptive Fourier Neural Operators*. Feb. 22, 2022. arXiv: 2202.11214 [physics]. URL: <http://arxiv.org/abs/2202.11214>. preprint.
- [26] Lu Lu et al. “Multifidelity Deep Neural Operators for Efficient Learning of Partial Differential Equations with Application to Fast Inverse Design of Nanoscale Heat Transport”. In: *Physical Review Research* 4.2 (June 13, 2022), p. 023210.
- [27] Shunyuan Mao et al. “PPDONet: Deep Operator Networks for Fast Prediction of Steady-state Solutions in Disk–Planet Systems”. In: *The Astrophysical Journal Letters* 950.2 (June 2023), p. L12.
- [28] Zongyi Li et al. *Fourier Neural Operator for Parametric Partial Differential Equations*. May 16, 2021. arXiv: 2010.08895 [cs, math]. URL: <http://arxiv.org/abs/2010.08895>. preprint.
- [29] Zongyi Li et al. “Physics-Informed Neural Operator for Learning Partial Differential Equations”. In: *ACM / IMS Journal of Data Science* 1.3 (May 20, 2024), 9:1–9:27.
- [30] Colin White et al. “Physics-Informed Neural Operators with Exact Differentiation on Arbitrary Geometries”. In: *The Symbiosis of Deep Learning and Differential Equations III*. Oct. 31, 2023.
- [31] Lu Lu et al. “Learning Nonlinear Operators via DeepONet Based on the Universal Approximation Theorem of Operators”. In: *Nature Machine Intelligence* 3.3 (3 Mar. 2021), pp. 218–229.
- [32] Sifan Wang, Hanwen Wang, and Paris Perdikaris. “Learning the Solution Operator of Parametric Partial Differential Equations with Physics-Informed DeepONets”. In: *Science Advances* 7.40 (Sept. 29, 2021), eabi8605.
- [33] Liu Yang et al. “In-Context Operator Learning with Data Prompts for Differential Equation Problems”. In: *Proceedings of the National Academy of Sciences* 120.39 (Sept. 26, 2023), e2310142120.
- [34] Thomas O’Leary-Roseberry et al. “Derivative-Informed Neural Operator: An Efficient Framework for High-Dimensional Parametric Derivative Learning”. In: *Journal of Computational Physics* 496 (Jan. 1, 2024), p. 112555.
- [35] Derick Nganyu Tanyu et al. “Deep Learning Methods for Partial Differential Equations and Related Parameter Identification Problems”. In: *Inverse Problems* 39.10 (Oct. 1, 2023), p. 103001.
- [36] Leon Herrmann and Stefan Kollmannsberger. “Deep Learning in Computational Mechanics: A Review”. In: *Computational Mechanics* (Jan. 13, 2024).

- [37] Steven L. Brunton and J. Nathan Kutz. *Machine Learning for Partial Differential Equations*. Mar. 29, 2023. arXiv: 2303.17078 [physics]. URL: <http://arxiv.org/abs/2303.17078>. preprint.
- [38] Aditi S. Krishnapriyan et al. *Characterizing Possible Failure Modes in Physics-Informed Neural Networks*. Nov. 11, 2021. arXiv: 2109.01050 [physics]. URL: <http://arxiv.org/abs/2109.01050>. preprint.
- [39] Yihua Zhang et al. *An Introduction to Bi-level Optimization: Foundations and Applications in Signal Processing and Machine Learning*. Dec. 20, 2023. arXiv: 2308.00788 [cs, math]. URL: <http://arxiv.org/abs/2308.00788>. preprint.
- [40] Shamsulhaq Basir and Inanc Senocak. *Critical Investigation of Failure Modes in Physics-informed Neural Networks*. June 28, 2022. arXiv: 2206.09961 [cs, math]. URL: <http://arxiv.org/abs/2206.09961>. preprint.
- [41] Diederik P. Kingma and Jimmy Ba. *Adam: A Method for Stochastic Optimization*. Jan. 29, 2017. arXiv: 1412.6980 [cs]. URL: <http://arxiv.org/abs/1412.6980>. preprint.
- [42] Sebastian Kaltenbach, Paris Perdikaris, and Phaedon-Stelios Koutsourelakis. *Semi-Supervised Invertible Neural Operators for Bayesian Inverse Problems*. Mar. 6, 2023. arXiv: 2209.02772 [physics, stat]. URL: <http://arxiv.org/abs/2209.02772>. preprint.
- [43] Tingtao Zhou et al. “AI-aided Geometric Design of Anti-Infection Catheters”. In: *Science Advances* 10.1 (Jan. 3, 2024), eadj1741.
- [44] Yan Yang et al. “Rapid Seismic Waveform Modeling and Inversion With Neural Operators”. In: *IEEE Transactions on Geoscience and Remote Sensing* 61 (2023), pp. 1–12.
- [45] Maarten V. de Hoop et al. *The Cost-Accuracy Trade-Off In Operator Learning With Neural Networks*. Aug. 11, 2022. arXiv: 2203.13181 [cs, math]. URL: <http://arxiv.org/abs/2203.13181>. preprint.
- [46] Lu Lu et al. “DeepXDE: A Deep Learning Library for Solving Differential Equations”. In: *SIAM Review* 63.1 (Jan. 2021), pp. 208–228.
- [47] Mohammad Amin Nabian, Rini Jasmine Gladstone, and Hadi Meidani. “Efficient Training of Physics-Informed Neural Networks via Importance Sampling”. In: *Computer-Aided Civil and Infrastructure Engineering* 36.8 (2021), pp. 962–977.
- [48] Chenxi Wu et al. “A Comprehensive Study of Non-Adaptive and Residual-Based Adaptive Sampling for Physics-Informed Neural Networks”. In: *Computer Methods in Applied Mechanics and Engineering* 403 (Jan. 1, 2023), p. 115671.
- [49] Sokratis J. Anagnostopoulos et al. “Residual-Based Attention in Physics-Informed Neural Networks”. In: *Computer Methods in Applied Mechanics and Engineering* 421 (Mar. 1, 2024), p. 116805.
- [50] Ameya D. Jagtap and George Em Karniadakis. “Adaptive Activation Functions Accelerate Convergence in Deep and Physics-Informed Neural Networks”. In: *Journal of Computational Physics* 404 (Mar. 2020), p. 109136. arXiv: 1906.01170 [physics].
- [51] Sifan Wang et al. *PirateNets: Physics-informed Deep Learning with Residual Adaptive Networks*. Feb. 11, 2024. arXiv: 2402.00326 [cs, math]. URL: <http://arxiv.org/abs/2402.00326>. preprint.
- [52] Sifan Wang, Yujun Teng, and Paris Perdikaris. “Understanding and Mitigating Gradient Flow Pathologies in Physics-Informed Neural Networks”. In: *SIAM Journal on Scientific Computing* 43.5 (Jan. 2021), A3055–A3081.
- [53] Ben Moseley, Andrew Markham, and Tarje Nissen-Meyer. “Finite Basis Physics-Informed Neural Networks (FBPINNs): A Scalable Domain Decomposition Approach for Solving Differential Equations”. In: *Advances in Computational Mathematics* 49.4 (July 31, 2023), p. 62.
- [54] Shamsulhaq Basir and Inanc Senocak. “Physics and Equality Constrained Artificial Neural Networks: Application to Forward and Inverse Problems with Multi-Fidelity Data Fusion”. In: *Journal of Computational Physics* 463 (Aug. 15, 2022), p. 111301.
- [55] Chuwei Wang et al. “Is L^2 Physics Informed Loss Always Suitable for Training Physics Informed Neural Network?” In: *Advances in Neural Information Processing Systems*. May 16, 2022.
- [56] Jeremy Yu et al. “Gradient-Enhanced Physics-Informed Neural Networks for Forward and Inverse PDE Problems”. In: *Computer Methods in Applied Mechanics and Engineering* 393 (Apr. 1, 2022), p. 114823.

- [57] Hwijae Son et al. *Sobolev Training for Physics Informed Neural Networks*. Dec. 8, 2021. arXiv: 2101.08932 [cs, math]. URL: <http://arxiv.org/abs/2101.08932>. preprint.
- [58] Suryanarayana Maddu et al. “Inverse Dirichlet Weighting Enables Reliable Training of Physics Informed Neural Networks”. In: *Machine Learning: Science and Technology* 3.1 (Feb. 2022), p. 015026.
- [59] Levi McClenny and Ulisses Braga-Neto. *Self-Adaptive Physics-Informed Neural Networks Using a Soft Attention Mechanism*. Apr. 5, 2022. arXiv: 2009.04544 [cs, stat]. URL: <http://arxiv.org/abs/2009.04544>. preprint.
- [60] Sifan Wang et al. *An Expert’s Guide to Training Physics-informed Neural Networks*. Aug. 16, 2023. arXiv: 2308.08468 [physics]. URL: <http://arxiv.org/abs/2308.08468>. preprint.
- [61] Zongren Zou, Xuhui Meng, and George Em Karniadakis. “Correcting Model Misspecification in Physics-Informed Neural Networks (PINNs)”. In: *Journal of Computational Physics* (Mar. 9, 2024), p. 112918.
- [62] K.R. Swanson, Jr. Alvord E.C., and J.D. Murray. “A Quantitative Model for Differential Motility of Gliomas in Grey and White Matter”. In: *Cell Proliferation* 33.5 (2000), pp. 317–329.
- [63] H.L.P. Harpold, E.C. Alvord Jr., and K.R. Swanson. “The Evolution of Mathematical Modeling of Glioma Proliferation and Invasion”. In: *Journal of Neuropathology and Experimental Neurology* 66.1 (2007), pp. 1–9.
- [64] Zhen Zhang et al. “Discovering a Reaction–Diffusion Model for Alzheimer’s Disease by Combining PINNs with Symbolic Regression”. In: *Computer Methods in Applied Mechanics and Engineering* 419 (Feb. 1, 2024), p. 116647.
- [65] Amelie Schäfer, Elizabeth C. Mormino, and Ellen Kuhl. “Network Diffusion Modeling Explains Longitudinal Tau PET Data”. In: *Frontiers in Neuroscience* 14 (2020).
- [66] Ivan Ezhov et al. “Learn-Morph-Infer: A New Way of Solving the Inverse Problem for Brain Tumor Modeling”. In: *Medical Image Analysis* 83 (Jan. 1, 2023), p. 102672.
- [67] Klaudius Scheufele, Shashank Subramanian, and George Biros. “Fully Automatic Calibration of Tumor-Growth Models Using a Single mpMRI Scan”. In: *IEEE Transactions on Medical Imaging* 40.1 (Jan. 2021), pp. 193–204.
- [68] Suchuan Dong and Naxian Ni. “A Method for Representing Periodic Functions and Enforcing Exactly Periodic Boundary Conditions with Deep Neural Networks”. In: *Journal of Computational Physics* 435 (June 15, 2021), p. 110242.
- [69] Lu Lu et al. “Physics-Informed Neural Networks with Hard Constraints for Inverse Design”. In: *SIAM Journal on Scientific Computing* 43.6 (Jan. 2021), B1105–B1132.
- [70] N. Sukumar and Ankit Srivastava. “Exact Imposition of Boundary Conditions with Distance Functions in Physics-Informed Deep Neural Networks”. In: *Computer Methods in Applied Mechanics and Engineering* 389 (Feb. 1, 2022), p. 114333.
- [71] Lawrence C. Evans. *Partial Differential Equations*. American Mathematical Soc., 2010. 778 pp. Google Books: Xnu0o_EJrCQC.
- [72] Lu Lu et al. “A Comprehensive and Fair Comparison of Two Neural Operators (with Practical Extensions) Based on FAIR Data”. In: *Computer Methods in Applied Mechanics and Engineering* 393 (Apr. 1, 2022), p. 114778.
- [73] Paul Constantine. *Random Field Simulation*. Version 1.5.0.0. MATLAB Central File Exchange, 2024.

Supplementary Material

In Appendix A, we provide the network architecture of the neural network used in the numerical experiments. In Appendix B, we provide a justification of the simultaneous gradient descent algorithm for the bi-level optimization problem. Appendix C provides the training detail and hyperparameters for the numerical experiments in Section 3.1 and 3.2 in the main text. In Appendix D, we compare BILO with solving PDE inverse problems using a neural operator. Appendix E includes numerical experiments, which includes

- E.1 Inferring a scalar coefficient in a nonlinear ODE problem
- E.2 Inferring the initial condition of a 1D heat equation
- E.3 Inferring the variable diffusion coefficient of a 2D Poisson problem

Appendix F shows the computational cost of BiLO.

A Network Architecture

The network architecture involves a simple modification at the input layer (embedding layer) of the typical fully connected neural network. For the scalar parameter case, the input layer maps the inputs \mathbf{x} and the unknown PDE parameters Θ to a high-dimensional vector \mathbf{y} , using an affine transformation followed by a non-linear activation function σ :

$$\mathbf{y} = \sigma(W\mathbf{x} + R\Theta + \mathbf{b}), \quad (22)$$

where W is the embedding matrix for \mathbf{x} , R is the embedding matrix for Θ , and \mathbf{b} is the bias vector. The key is that the embedding matrix R should be non-trainable. Otherwise, $\mathcal{L}_{\text{rgrad}}(W, \Theta)$ can be made 0 by setting R to be 0. In our work, R will be randomly initialized in the same way as W , using uniform distributions in the range of $[-1/\sqrt{d}, 1/\sqrt{d}]$, where d is the number of input units in the layer. The embedding vector \mathbf{y} is then passed through a series of fully connected layers with activation functions. The output of the network is denoted as $\mathcal{N}(\mathbf{x}, \Theta; W)$, where W denotes all the trainable weights of the neural network. In some cases, a final transformation is applied to the output of the neural network $u(\mathbf{x}; W) = \tau(\mathcal{N}(\mathbf{x}, \Theta; W), \mathbf{x})$, to enforce the boundary condition [68–70].

B Simultaneous Gradient Descent

In the main text, we describe the simultaneous gradient descent algorithm for the bi-level optimization problem. In this section, we provide a justification of the algorithm under some assumptions.

We consider the boundary value problem:

$$\begin{cases} \mathbf{L}u = f & \text{in } \Omega \\ u = g & \text{on } \partial\Omega, \end{cases} \quad (23)$$

where Ω is an connected, open and bounded subset of \mathbb{R}^d . \mathbf{L} denoteds a second-order parital differential operator:

$$\mathbf{L}u = \sum_{i,j=1}^d a_{ij} \partial_{ij} u + \sum_{i=1}^d b_i \partial_i u + cu \quad (24)$$

where the coefficients a_{ij} , b_i , c are colletively denoted as Θ . We denote \mathbf{L}_Θ as the derivative of \mathbf{L} with respect to Θ , which is also a differential operator.

We say a function $u(\mathbf{x}, \Theta)$ is a local solution operator of the PDE (24) at Θ if (1) $\mathbf{L}u = f$ and (2) $L_\Theta u + L\nabla_\Theta u = 0$. That is, the residual at Θ is zero and the gradient of the residual w.r.t Θ is zero.

We consider a parameterized local operator $u(\mathbf{x}, \Theta; W)$. For notational simplicity, we omit the dependence of u on \mathbf{x} in the following discussion. We assume that $u(\Theta; W) = g$ on $\partial\Omega$ for all W and Θ .

Our bilevel optimizaiton problem is

$$\min_{\Theta} \int_{\Omega} (u(\Theta, W^*(\Theta)) - \hat{u})^2 dx$$

$$W^*(\Theta) = \arg \min \int_{\Omega} (\mathbf{L}u - f)^2 + w_{\text{reg}} (L_{\Theta}u + L\nabla_{\Theta}u)^2 dx$$

where $\mathbf{L}u - f$ is the residual of the PDE, and $L_{\Theta}u + L\nabla_{\Theta}u$ is the gradient of the residual w.r.t Θ .

In our simultaneous gradient descent, the gradient of the upper level objective with respect to Θ is given by

$$g_a(W, \Theta) = \int_{\Omega} (u(W, \Theta) - \hat{u}) (\nabla_{\Theta}u(W, \Theta)) dx \quad (25)$$

The exact gradient of the upper level objective is

$$g(\Theta) = \int_{\Omega} (u(W^*(\Theta), \Theta) - \hat{u}) (\nabla_W u(W^*(\Theta), \Theta) \nabla_{\Theta} W^*(\Theta) + \nabla_{\Theta} u(W^*(\Theta), \Theta)) dx \quad (26)$$

At $W^*(\Theta)$, the difference between the exact gradient and the approximate gradient, which we denote as Δg , is given by

$$\begin{aligned} \Delta g(\Theta) &:= g_a(W^*(\Theta), \Theta) - g(\Theta) \\ &= \int_{\Omega} (u(W^*(\Theta), \Theta) - \hat{u}) (\nabla_W u(W^*(\Theta), \Theta) \nabla_{\Theta} W^*(\Theta)) dx \end{aligned} \quad (27)$$

Suppose the lower level problem has a minimizer $W^*(\Theta)$ such that the $u(W^*(\Theta), \Theta)$ is the local operator.

$$\mathbf{L}u(W^*(\Theta), \Theta) - f = 0 \quad (28)$$

and

$$\mathbf{L}_{\Theta}u(W^*(\Theta), \Theta) + \mathbf{L}\nabla_{\Theta}u(W^*(\Theta), \Theta) = 0 \quad (29)$$

Take the derivative of the Eq. (28) with respect to Θ , we have

$$\mathbf{L}_{\Theta}u(W^*(\Theta), \Theta) + \mathbf{L}\nabla_{\Theta}u(W^*(\Theta), \Theta) + \mathbf{L}\nabla_W u(W^*(\Theta), \Theta) \nabla_{\Theta} W^*(\Theta) = 0 \quad (30)$$

From Eq. (29) and Eq. (30), we have

$$\mathbf{L}\nabla_W u(W^*(\Theta), \Theta) \nabla_{\Theta} W^*(\Theta) = 0 \quad (31)$$

We denote the function $v := \nabla_W u(W^*(\Theta), \Theta) \nabla_{\Theta} W^*(\Theta)$. Since $u(W, \Theta) = g$ on $\partial\Omega$ for all W and Θ , we have $v = 0$ on $\partial\Omega$. Therefore, we have $\mathbf{L}v = 0$ in Ω and $v = 0$ on $\partial\Omega$. If the maximum principal holds for the operator \mathbf{L} , for example, when \mathbf{L} uniformly elliptic and $c \geq 0$, [71] then we have $v = 0$.

By Cauchy-Schwarz inequality, we have

$$\|\Delta g\|_2 \leq \|u(W^*(\Theta), \Theta) - \hat{u}\|_2 \|v\|_2 = 0 \quad (32)$$

That is, the approximate gradient at $W^*(\Theta)$ is exact.

We summarize the above discussion in the following proposition:

Proposition: Assuming (i) the maximum principal holds for \mathbf{L} ; (ii) the parametrized local operator $u(W, \Theta) = g$ on $\partial\Omega$ for all W and Θ ; (iii) the lower level problem has a minimizer $W^*(\Theta)$ such that the $u(W^*(\Theta), \Theta)$ is the local operator, then the approximate gradient (25) of the upper level objective at $W^*(\Theta)$ is exact.

The assumptions are more restrictive than the numerical experiments. For example, in the Fisher-KPP example, the PDE operator is nonlinear. A more comprehensive and general analysis is left for future work.

C Training Details

For each numerical experiment, we solve the optimization problem 5 times with different random seed, which affect both the initialization of the neural network and the noise in the data (if applicable). Although each realization of the noise may yield a different optimal parameter Θ^* , the average of the optimal parameters across multiple runs should still be close to the ground truth parameter Θ_{GT} . Therefore, we report the mean and standard deviation of the error between the inferred parameters, or functions, and the ground truth quantities.

In all the numerical experiment, we use the tanh activation function and 2 hidden layers, each with 128 neurons, for both PINN and BiLO. The collocation points are evenly spaced as a grid in the domain. For all the optimization problems, we use the Adam optimizer with learning rate 0.001 and run a fixed number of steps.

Fisher-KPP Equation Our local operator take the form of $u(x, t, D, \rho; W) = u(x, 0) + \mathcal{N}(x, t, D, \rho; W)x(1-x)t$ so that the initial condition and the boundary condition are satisfied. Let X_r, X_d be the spatial coordinates evenly spaced in $[0, 1]$, and T_r be temporal coordinates evenly spaced in $[0, 1]$. We set $\mathcal{T}_{res} = X_r \times T_r$ and $|X_r| = |T_r| = 21$, that is, the residual collocation points are a uniform grid in space and time. We set $\mathcal{T}_{dat} = X_d \times \{1\}$ and $|X_d| = 11$, that is, the data collocation points form a uniform grid at the final time $t = 1$. Both BiLO and PINN are pretrained with the initial guess for 10,000 steps, and fine-tuned for 10,000 steps.

In Fig. 4, we show an example of the training history of the losses and the inferred parameters corresponding to Fig 2, and indicate the ground truth with grey dashed line. For data loss, the ground truth solution should have a data loss of $1e-4$, which is the variance of the noise.

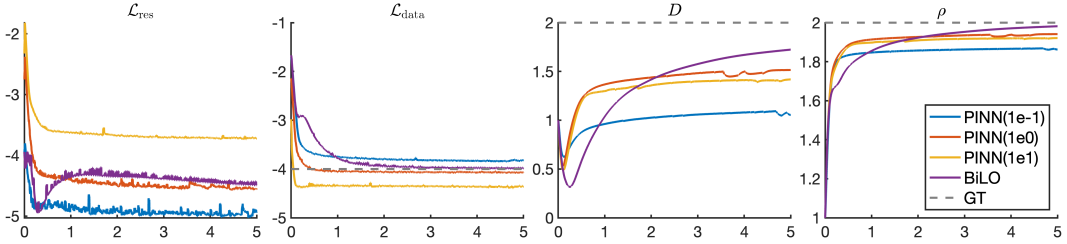


Figure 4: Training history of losses and the inferred parameters corresponding to Fig 2. The losses are in log scale.

Poisson Equation with Variable Diffusion Coefficient The local operator takes the form of $u(x, z; W) = \mathcal{N}_1(x, z; W)x(1-x)$ to enforce the boundary condition, where the fully connected neural network \mathcal{N}_1 has 2 hidden layers, each with 128 neurons. The unknown function is parameterized by $D(x; V) = \mathcal{N}_2(x, V)x(1-x) + 1$, where \mathcal{N}_2 has 2 hidden layers, each with 64 neurons. For pre-training, we set $|\mathcal{T}_{res}| = |\mathcal{T}_{reg}| = |\mathcal{T}_{dat}| = 101$, and train 10,000 steps. For fine-tuning, we set $|\mathcal{T}_{res}| = |\mathcal{T}_{reg}| = 101$ and $|\mathcal{T}_{dat}| = 51$, and train 10,000 steps.

D Comparison with Neural Operators

In this section, we compare the results of BiLO and Neural Operators (NO) for solving the inverse problems. For the NO, we use the DeepONet architecture [31] as an example, which is shown to have comparable performance with FNO [28, 72].

It is difficult to directly compare the performance of NO and PINN/BiLO, since NOs are designed to learn the solution operator of the PDE, while both the PINN and BiLO can be considered as the solver of the PDE, which solve the PDE for one set of parameters. Ususally, NO is trained with a large amount of numerical solutions. In this experiment, for solving the inverse problem, we first train the NO, and then we use the NO as a surrogate and use gradient-based optimization to infer the parameters of the PDE. We show the the quality of the inferred parameters depends on the quality of the synthetic data used to train the NO.

We emphasize that NO can excel in multi-query scenarios, such as solving the inverse problem in a Bayesian framework, which requires evaluating the solution of the PDE for many different parameters.

D.1 Fisher-KPP Equation

In this experiment, we consider the Fisher-KPP equation with noise, as in Section. 3.1. We consider the following 3 datasets for pretraining the DeepONet. The ground truth parameters are $D_{GT} = 2$ and $\rho_{GT} = 2$, and the initial guess is $D_0 = 1$ and $\rho_0 = 1$. The PDE parameters are sampled with different range and different resolution. We use the notation $a : h : b$ to denote an array from a to b with step h .

- Coarse: $D = 0.8 : 0.05 : 3, \rho = 0.8 : 0.05 : 3$.
- Dense: $D = 0.8 : 0.02 : 3, \rho = 0.8 : 0.02 : 3$.
- Out-of-distribution (OOD): $D = 0.8 : 0.02 : 1.8, \rho = 0.8 : 0.02 : 1.8$.

In the ‘‘Coarse’’ dataset, the parameters are sampled with a larger step size. In the ‘‘Dense’’ dataset, the parameters are sampled with a smaller step size. In the ‘‘OOD’’ dataset, the parameters are sampled with a smaller step size, does not include the ground truth parameters.

We use the following architecture for the DeepONet:

$$G_W(D, \rho, \mathbf{x}) = \sum_{i=1}^k b_k(D, \rho) t_k(\mathbf{x})$$

where $b_k(D, \rho)$ is the k -th output of the ‘‘branch net’’, and $t_k(\mathbf{x})$ is the k -th output of the ‘‘truck net’’. Both the trunk net and the truck net are parameterized by fully neural networks with 2 hidden layers, each with 128 neurons, so that the total number of parameters (46179) are comparable to the network used by BiLO (42051). The weights of the DeepONet are denoted as W . A final transformation on the output G_W is used to enforce the boundary condition. We pre-train multiple DeepONets with 10,000 steps using each datasets.

Given a pretrain dataset with collections of $\{D^j, \rho^j\}$ and their corresponding solutions u^j for $j = 1, \dots, m$, we first train the DeepONet with the following operator data loss:

$$\min_W \sum_{j=1}^m \sum_{\mathbf{x} \in \mathcal{T}_{\text{dat}}} |G_W(D^j, \rho^j, \mathbf{x}) - u^j(\mathbf{x})|^2$$

where \mathcal{T}_{dat} is the same as those used in the BiLO and PINN. For the inverse problem, we fix the weights W and treat the D and ρ as unknown variables. We minimize the data loss:

$$\min_{D, \rho} \frac{1}{|\mathcal{T}_{\text{dat}}|} \sum_{\mathbf{x} \in \mathcal{T}_{\text{dat}}} |G_W(D, \rho, \mathbf{x}) - \hat{u}(\mathbf{x})|^2$$

where \hat{u} is the noisy data.

As shown in Table 1 in the main text, the performance of the inference depends on properties of the pre-training dataset. When the ground truth is out of the distribution of the pre-training dataset, the DeepONet gives poor performance.

D.2 Variable-Diffusion Coefficient Poisson Equation

In this experiment, we infer the variable diffusion coefficient $D(x)$ in the Poisson equation using a DeepONet. The pretrain dataset is generated by solving the Poisson equation with 1000 samples of variable diffusion coefficient $D(x)$. $D(x)$ is sampled from a Gaussina Random field on $[0, 1]$, conditioned on $D(0) = D(1) = 1$. The covariance function is the gaussian kernel, with variance 0.05 and different length scale $l = 0.2, 0.3, 0.4$. See Figure 5 for the samples of $D(x)$ and their corresponding solutions. As l increases, the samples of $D(x)$ become smoother.

The DeepONet has the following architecture:

$$G_W(\mathbf{D}, \mathbf{x}) = \sum_{i=1}^k b_k(\mathbf{D}) t_k(\mathbf{x})$$

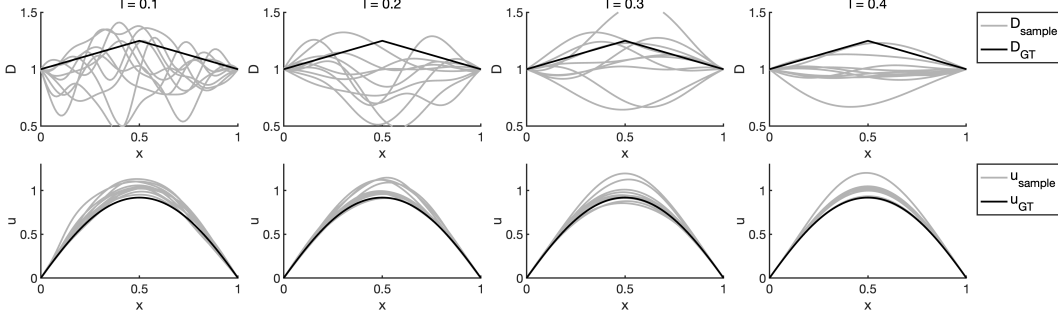


Figure 5: Samples (gray lines) of $D(x)$ with various length scale l and their corresponding solutions. Black line is the ground truth D and u

where the vector \mathbf{D} represent the values of $D(x)$ at the collocation points. A final transformation on the output G_W is used to enforce the boundary condition. In this experiment, both D and u are evaluated at 101 points in $[0, 1]$. Let x_i be the collocation points in $[0, 1]$ for $i = 1, \dots, N$. Let $\{D^j(x_i), u^j(x_i)\}$ be the samples of D and the corresponding solutions u at x_i for $j = 1, \dots, m$. We denote \mathbf{D}^j as the vector of $D^j(x_i)$ for $i = 1, \dots, N$. In the pre-training step, we solve the following minimization problem

$$\min_W \sum_{j=1}^m \sum_{i=1}^N |G_W(\mathbf{D}^j, x_i) - u^j(x_i)|^2$$

For the inverse problem, we fix the weights W and treat the \mathbf{D} as an unknown variable. We minimize the data loss and a finite difference discretizations of the regularization term $|D(x)|^2$:

$$\min_{\mathbf{D}} \frac{1}{N} \sum_{i=1}^N |G_W(\mathbf{D}, x_i) - \hat{u}(x_i)|^2 + w_{\text{reg}} \sum_{i=1}^{N-1} |(\mathbf{D}_{i+1} - \mathbf{D}_i)/h|^2$$

where h is the spacing of the collocation points. Here we work with the vector \mathbf{D} for simplicity. Alternatively, we can represent $D(x)$ as a neural network as in PINN and BiLO experiments.

We perform a grid search on the hyperparameters $l = 0.1, 0.2, 0.3, 0.4$ and $w_{\text{reg}} = 1e-3, 1e-4, 1e-5$. In Table 3, we show the 3 combinations of l and w_{reg} with the best performance in terms of the L_2 error of the inferred $D(x)$ and the ground truth. As shown in Table 3, the performance of the inference depends on properties of the pre-training dataset. In practice, it might be difficult to know what does the ground truth unknown function look like. This highlights the importance of the residual loss used in BiLO and PINN, which can help to learn the solution of the PDE without prior knowledge of the ground truth solution.

method	$\ D - D_{GT}\ _{\infty}$	$\ D - D_{GT}\ _2$	$\ u_{\text{NN}} - u_{\text{FDM}}\ _{\infty}$	$\mathcal{L}_{\text{data}}$
BiLO	$5.86e-2 \pm 1.99e-2$	$2.01e-2 \pm 7.94e-3$	$3.94e-3 \pm 1.93e-3$	$1.01e-4 \pm 1.80e-5$
DeepONet(0.2/1e-5)	$5.55e-2 \pm 7.99e-3$	$2.36e-2 \pm 2.05e-3$	$6.56e-3 \pm 2.36e-3$	$9.45e-5 \pm 1.47e-5$
DeepONet(0.4/1e-5)	$6.83e-2 \pm 2.76e-2$	$2.94e-2 \pm 1.14e-2$	$8.65e-3 \pm 9.37e-4$	$8.62e-5 \pm 1.36e-5$
DeepONet(0.4/1e-4)	$8.22e-2 \pm 2.08e-2$	$3.16e-2 \pm 8.63e-3$	$7.73e-3 \pm 1.89e-3$	$1.01e-4 \pm 1.83e-5$

Table 3: Comparison of BiLO and DeepONets (l / w_{reg}) pre-trained with datasets with different length scale l and regularization weight w_{reg} .

E Additional Numerical Experiments

E.1 Nonlinear System of ODEs

In this example, we consider inferring the unknown parameter a in the following system of ODEs:

$$\begin{cases} \frac{\partial u_1}{\partial t} = 0.2u_1^3 + 4u_2^3 \\ \frac{\partial u_2}{\partial t} = au_1^3 - 0.2u_2^3 \end{cases} \quad (33)$$

with initial condition $u_1(0) = 1$, $u_2(0) = 0$ and $t \in [0, 1]$. We set the ground truth $a_{\text{GT}} = -4$ and take $a_0 = -2$ as the initial guess. To enforce the initial condition, the network have the form $u(t, a; W) = \mathcal{N}(t, a; W)t + u_0$, where u_0 is the initial condition (similar for the PINNs). We set $|\mathcal{T}_{\text{res}}| = |\mathcal{T}_{\text{dat}}| = 11$ and train for 20,000 steps.

Effect of residual-gradient loss In Fig. 6, we visualize the function $u(t, a_0 + \delta a; W)$ after pre-training with $a_0 = -2$ for $\delta a = 0, -0.2, 0.2$. We can see that the neural network approximate the solution of the ODE for small variation of a .

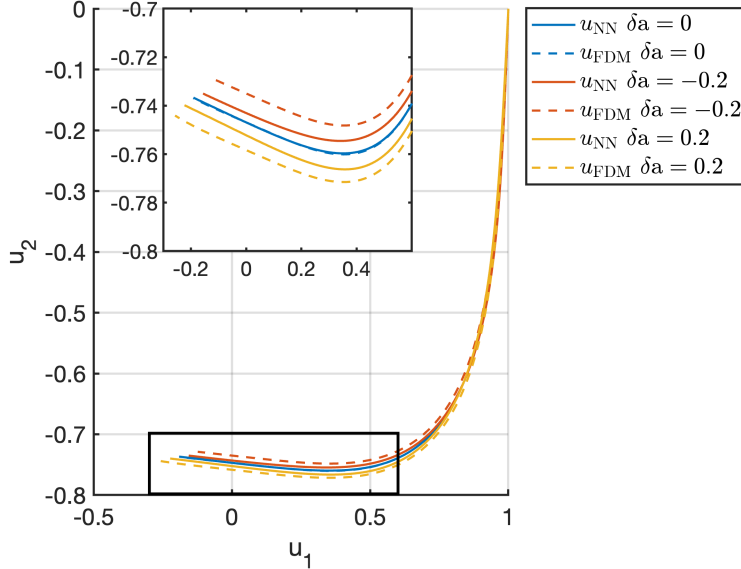


Figure 6: Evaluating $u(t, a_0 + \delta a; W)$ after pre-training with $a_0 = -2$. The network approximates the solution of the ODE for small variation of a .

Inference with Noise Data In Table 4, we show the inference results for the ODE problem with noise $\epsilon \sim N(0, 0.05)$. We compare the performance of the PINNs with various w_{dat} and BiLO. For the PINNs, as w_{dat} increase from $1e-3$ to $1e1$, the accuracy of the inferred parameter a decreases and increases. As w_{dat} goes above $1e-1$, we can see the network tends to over-fit the data, as \mathcal{L}_{dat} gets smaller than the variance of the noise, and \mathcal{L}_{res} gets larger, while BiLO gives more accurate inferred parameter and ODE solution. In Fig. 7, we show one instance of 5 random trials to compare the results of the PINN formulation with different pairs of weights $w_{\text{dat}}=0.1, 1, 10$, and BiLO.

method	$ a_{\text{pred}} - a_{\text{GT}} $	$\mathcal{L}_{\text{data}}$	$\ u_{\text{NN}} - u_{\text{FDM}}\ _{\infty}$
BiLO	0.23 ± 0.18	$5.04e-2 \pm 1.28e-2$	$1.10e-1 \pm 8.31e-2$
PINN($1e-2$)	0.31 ± 0.16	$5.41e-2 \pm 1.05e-2$	$1.48e-1 \pm 7.60e-2$
PINN($1e-1$)	0.33 ± 0.40	$4.49e-2 \pm 1.13e-2$	$7.17e-2 \pm 5.81e-2$
PINN($1e0$)	1.39 ± 0.76	$1.71e-2 \pm 1.07e-2$	$3.37e-1 \pm 1.52e-1$

Table 4: Comparison of BiLO and PINNs (with various w_{dat}) for a nonlinear ODE problem with noise ($\epsilon \sim N(0, 0.04)$): mean (std) for predicted a deviation from ground truth ($a_{\text{GT}} = -4$) and losses L_r and L_d

E.2 Infer the Initial Condition of a Heat Equation

In this example, we aim to infer the initial condition of a 1D heat equation from the final state. Consider the heat equation

$$\begin{cases} u_t(x, t) = Du_{xx}(x, t) \\ u(x, 0) = f(x) \\ u(0, t) = u(1, t) = 0 \end{cases} \quad (34)$$

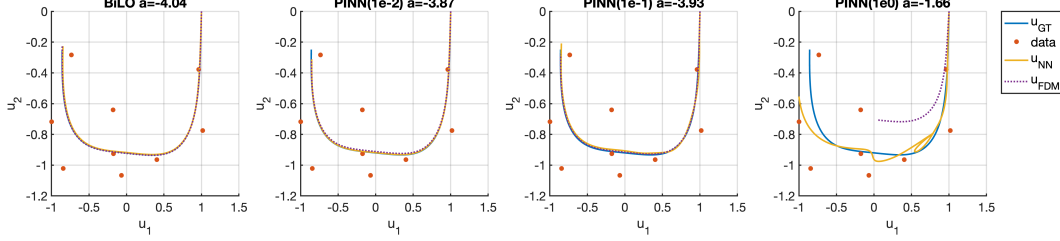


Figure 7: Network predicted solutions u_{NN} (BiLO and PINNs with different w_{dat}) and FDM solution u_{FDM} with the inferred parameter a .

on $x \in [0, 1]$ and $t \in [0, 1]$, with fixed diffusion coefficient $D = 0.01$, and unknown initial condition $f(x)$, where $f(0) = f(1) = 0$. Our goal is to infer the initial condition $f(x)$ from observation of the final state $u(x, 1)$. We set the ground truth initial condition f_{GT} to be the hat function

$$f_{\text{GT}}(x) = \begin{cases} 2x, & \text{if } x \in [0, 0.5) \\ 2 - 2x, & \text{if } x \in [0.5, 1] \end{cases} \quad (35)$$

We set the initial guess $f_0(x) = \sin(\pi x)$. We can represent the unknown function $f(x; V) = s(\mathcal{N}(x; V))x(1-x)$, where \mathcal{N}_f is a fully connected neural network with 2 hidden layers and width 64, and s is the softplus activation function (i.e., $s(x) = \log(1 + \exp(x))$). The transformation ensures that the initial condition satisfies the boundary condition and is non-negative. For BiLO, the neural network is represented as $u(x, t, z) = N_u(x, t, z; W)x(1-x)t + z$, where N_u is a fully connected neural network with 2 hidden layers and width 128. For the PINN, we have $u(x, t; W, V) = N_u(x, t; W)x(1-x)t + f(x; V)$. These transformations ensure that the networks satisfy the boundary and initial condition.

Let X_r, X_d be spatial coordinates evenly spaced in $[0, 1]$ and T_r be temporal coordinates evenly spaced in $[0, 1]$ (both including the boundary). We set $\mathcal{T}_{\text{res}} = X_r \times T_r$ and $|X_r| = |T_r| = 51$. That is, the residual collocation points is a uniform grid in space and time. We set $\mathcal{T}_{\text{dat}} = X_d \times \{1\}$ and $|X_d| = 11$. That is, the data collocation points is a uniform grid in space at the final time $t = 1$. We set the collocation point for the regularization loss of the unknown function \mathcal{T}_{reg} to be 101 evenly spaced points in the spatial domain.

To evaluate the performance of the inferred initial condition f , we use the L_2 norm and the L_∞ norm of the difference between the inferred initial condition and the ground truth initial condition, which are evaluated at 1001 evenly spaced points in the spatial domain.

Without Noise

First we consider the case where the data is provided at $t = 1$ without noise. In this case, we also do not use regularization term for the initial condition. In Fig. 8, and Table 5, we show the results of PINNs various weights $w_{\text{dat}} = 0.1, 10, 1000$, and BiLO. We can see that BiLO achieved the best e_2 and e_∞ , demonstrating the effectiveness in recovering the non-smooth initial condition. With very large data loss, the error of the PINN increases. This is because data is only provided at the final time, we need to solve the PDE accurately to infer the initial condition.

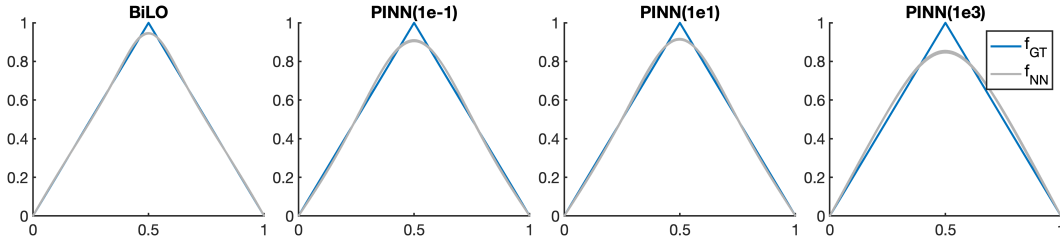


Figure 8: Predicted initial conditions of the heat equation (without noise) from 5 random seeds.

method	$\ f_{\text{NN}} - f_{\text{GT}}\ _{\infty}$	$\ f_{\text{NN}} - f_{\text{GT}}\ _2$	$\ u_{\text{NN}} - u_{\text{FDM}}\ _{\infty}$	$\mathcal{L}_{\text{data}}$
BiLO	5.43e-2±1.00e-3	1.01e-4±7.46e-6	4.64e-4±2.57e-4	1.52e-9±5.89e-10
PINN(1e-1)	9.24e-2±2.21e-3	5.43e-4±2.81e-5	1.29e-3±1.53e-3	4.05e-6±4.57e-6
PINN(1e1)	8.69e-2±2.39e-3	4.31e-4±5.06e-5	2.44e-3±9.86e-4	1.62e-6±1.82e-6
PINN(1e3)	1.49e-1±4.19e-3	1.92e-3±1.34e-4	2.54e-2±2.92e-3	3.83e-8±5.36e-8

Table 5: Comparison of BiLO and PINNs (with various w_{dat}) for inferring the unknown initial condition (without noise), showing mean (std).

With Noise

In this experiment, we consider the case with noise $\epsilon \sim N(0, 0.001)$. Due to the ill-posedness of the inverse problem, we need to regularize the problem by the 2-norm of the derivative of the unknown function with $w_{\text{reg}} = 1e - 2$. In Fig. 9 and Table 6, we show examples of the inferred initial condition and the PDE solution for the PINN formulation with various w_{dat} . In Table 6, for the PINN, we can see that as w_{dat} increase from 0.1 to 10, it seems that the reconstruction error decreases. However, the \mathcal{L}_{dat} is becoming smaller than the variance of the noise, indicating that the PINN is overfitting the data. This can also be observed from the Fig 9, for $w_{\text{dat}} = 1e3$, we see larger discrepancy between u_{PINN} and u_{FDM} .

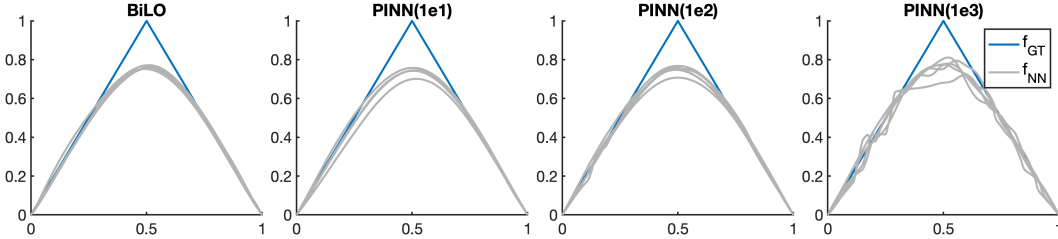


Figure 9: Predicted initial condition $f(x)$ by BiLO and PINNs with various w_{dat} .

method	$\ f_{\text{NN}} - f_{\text{GT}}\ _{\infty}$	$\ f_{\text{NN}} - f_{\text{GT}}\ _2$	$\ u_{\text{NN}} - u_{\text{FDM}}\ _{\infty}$	$\mathcal{L}_{\text{data}}$
BiLO	2.41e-1±7.62e-3	6.11e-3±5.36e-4	1.46e-3±7.50e-4	4.08e-3±2.53e-4
PINN(1e1)	2.62e-1±2.22e-2	8.13e-3±2.79e-3	1.26e-1±3.27e-2	5.21e-4±1.55e-4
PINN(1e2)	2.53e-1±2.34e-2	7.11e-3±2.06e-3	1.38e-1±3.17e-2	2.61e-4±1.56e-4
PINN(1e3)	2.42e-1±4.65e-2	6.56e-3±2.70e-3	1.36e-1±3.33e-2	2.05e-4±1.65e-4

Table 6: Comparison of the BiLO and PINN (with various w_{dat}) for a heat equation with unknown initial condition (noise $\epsilon \sim N(0, 0.001)$), showing mean (std).

E.3 2D Poisson Equation with Variable Diffusion Coefficient

The setup of this experiment is similar to the steady state Darcy flow inverse problem in [29]. We consider the following 2D Poisson equation with variable diffusion coefficient in the unit square domain $\Omega = [0, 1] \times [0, 1]$ with Dirichlet boundary condition:

$$\begin{cases} -\nabla \cdot (A(\mathbf{x})\nabla u(\mathbf{x})) = f(\mathbf{x}) & \text{in } \Omega \\ u(\mathbf{x}) = 0, & \text{on } \partial\Omega \end{cases} \quad (36)$$

Our goal is to infer the variable diffusion coefficient $A(\mathbf{x})$ from the solution $u(\mathbf{x})$.

Let $\phi(\mathbf{x})$ be samples of a Gaussian random field (GRF) with mean 0 and squared exponential (Gaussian) covariance structure $C(\mathbf{x}, \mathbf{y}) = \sigma \exp(-\|\mathbf{x} - \mathbf{y}\|^2/\lambda^2)$, where the marginal standard deviation $\sigma = \sqrt{10}$ and the correlation length $l = 0.01$ [73]. This GRF is different from [29]. We generate the initial guess $A_0(\mathbf{x}) = \text{sigmoid}(\phi_0(\mathbf{x})) \times 9 + 3$, where $\phi_0(\mathbf{x})$ is a sample of the GRF. We consider the ground truth diffusion coefficient to be a piece-wise constant function: $A_{\text{GT}}(\mathbf{x}) = 12$ if $\phi_{\text{GT}}(\mathbf{x}) > 0$ and $A_{\text{GT}}(\mathbf{x}) = 3$ otherwise, where ϕ_{GT} is another sample of the GRF. The corresponding solution of A_0 and A_{GT} are denoted as u_0 and u_{GT} .

We pretrain the BiLO with $A_0(\mathbf{x})$ and its corresponding solution $u_0(\mathbf{x})$ for 10,000 steps. And we fine-tune the BiLO for 5,000 steps using $u_{GT}(\mathbf{x})$ to infer A_{GT} . Following [29], we use the total variation regularization $|\nabla A|$ with weight $w_{reg} = 1e - 9$.

The unknown function is represented $A(\mathbf{x}; V) = s(\mathcal{N}(\mathbf{x}; V)) \times 9 + 3$, where N_f is a fully connected neural network with 2 hidden layers and width 64, and s is the sigmoid activation function (i.e., $s(u) = 1/(1 + \exp(-u))$). The transformation is a smoothed approximation of the piece-wise constant function. For BiLO, the neural network is represented as $u(\mathbf{x}, z) = N_u(\mathbf{x}, z; W) \mathbf{x}_1(1 - \mathbf{x}_1) \mathbf{x}_2(1 - \mathbf{x}_2)$, where N_u is a fully connected neural network with 2 hidden layers and width 128, and z is our auxiliary variable such that $z = A(\mathbf{x}; V)$.

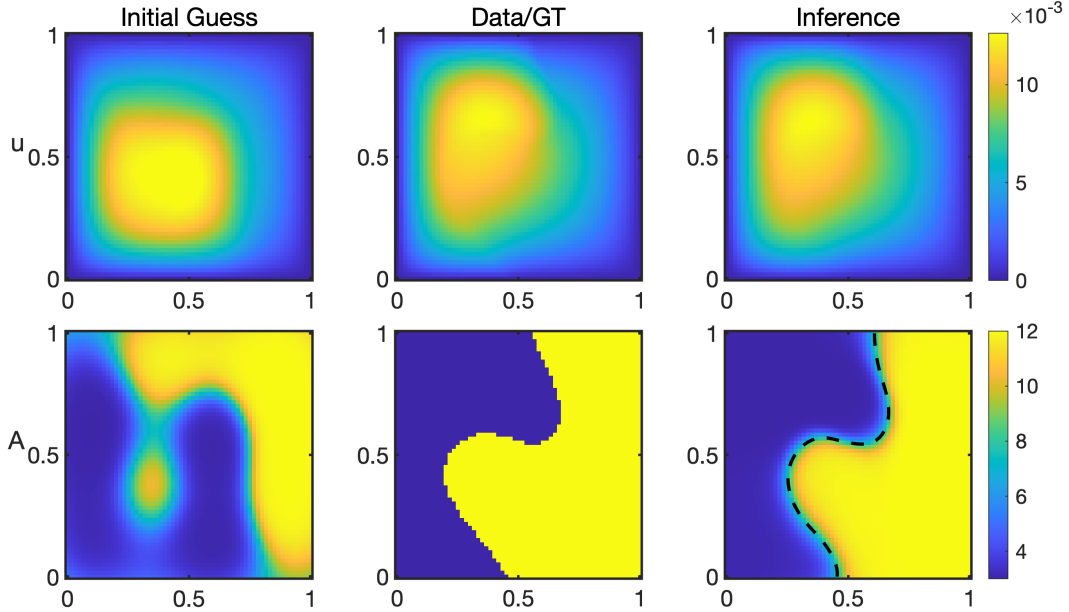


Figure 10: Example 1 of inferring the variable diffusion coefficient. The relative l2 error of u_{NN} against u_{GT} is 1.3%. The thresholded (at the dashed line) inferred diffusion coefficient has classification accuracy of 98%

In Figure 10 and Figure 11, we show two examples of the results, each with different initial guess A_0 and ground truth A_{GT} . In example 1 (see Figure 10), the relative error of the inferred diffusion coefficient is 1.3%. If we threshold the inferred diffusion coefficient at 7.5 (the mid-point of 3 and 12), the classification accuracy is 98%. In example 2 (see Figure 11), the relative error of the inferred diffusion coefficient is 1.7%. If we threshold the inferred diffusion coefficient, the classification accuracy is 96%. Our performance is comparable to the results (2.29% relative l2 error on u and 97.10% classification accuracy) from the Physics-informed Neural Operator (PINO) in [29], which require pretraining a FNO with synthetic dataset, and instance-wise fine-tuning with physics-informed loss. For our method, we only need to pretrain the BiLO with a single initial guess. In addition, as shown in the figures, the initial guess can be very different from the ground truth.

F Computational Cost

Compared with PINN, BiLO involve computing a higher order derivative term in the residual-gradient loss. This increases the memory cost and computation time per step. However, as shown in Fig. 4, BiLO might require fewer iterations to achieve certain accuracy of the parameters.

In Table. 7, we show the seconds-per-step and the maximum memory allocation of 1 run of BiLO and PINN for the various problems. The seconds per step is computed by total training time divided by the number of steps. The maximum memory allocation is the peak memory usage during the training. For all the experiments, we use Quadro RTX 8000 GPU. We note that the measured seconds-per-step is not subject to rigorous control as the GPU is shared with other users and many

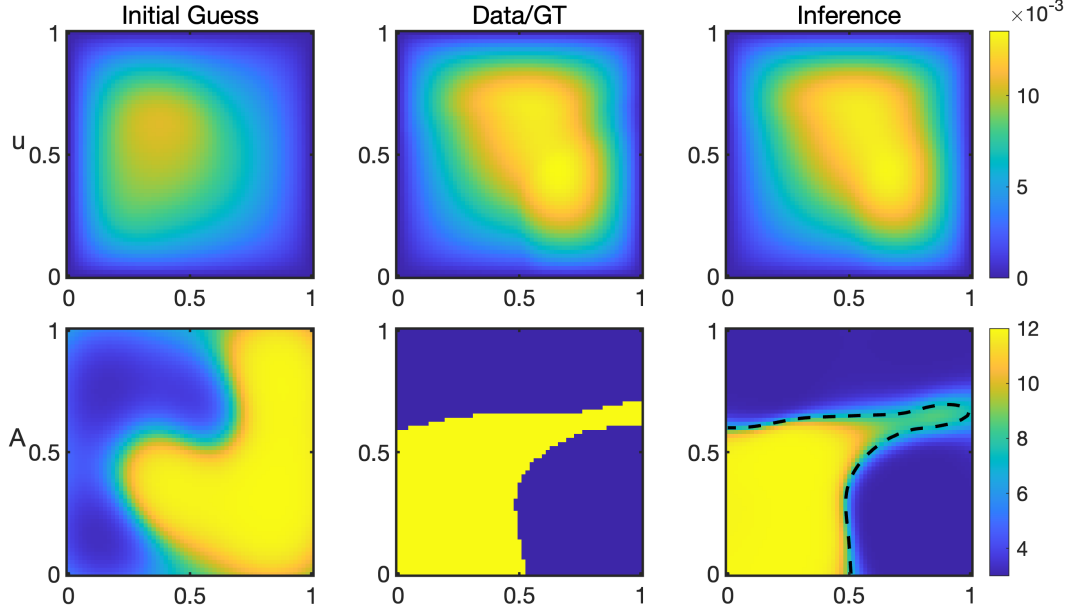


Figure 11: Example 2 of inferring the variable diffusion coefficient. The relative l2 error of u_{NN} against u_{GT} is 1.7%. The thresholded (at the dashed line) inferred diffusion coefficient has classification accuracy of 96%

runs are performed simultaneously. Detailed study of the computational efficiency of BiLO will be left for future work.

Problem	Metric	BiLO	PINN	BiLO/PINN
Fisher-KPP	sec-per-step	0.13	0.086	1.51
	max-mem-alloc	437	105	4.16
Nonlinear ODE	sec-per-step	0.05	0.024	2.08
	max-mem-alloc	18.6	17.9	1.04
1D Poisson	sec-per-step	0.05	0.03	1.67
	max-mem-alloc	30	22	1.36
Heat	sec-per-step	0.096	0.06	1.60
	max-mem-alloc	367	171	2.15

Table 7: Example of computational cost of BiLO and PINN and their ratio for various problems.

It is not straightforward to comparing the computational cost with Neural operators. Neural operators can be very fast in the inference stage (solving inverse problem). However, they have significant overhead, which involve preparing the training data, that is, solve the PDE numerically for a large collection of parameters, and pre-train the neural network. The overall cost might be favorable in the many-query settings. However, if we aim to solve the inverse problem once, the total computational cost might not be favorable.